ADVANCED ENERGY MATERIALS
www.advenergymat.de



# Charge Pumping Strategy for Rotation and Sliding Type Triboelectric Nanogenerators

*Yu Bai, Liang Xu, Shiquan Lin, Jianjun Luo, Huaifang Qin, Kai Han, and Zhong Lin Wang**

**Triboelectric nanogenerator (TENG) is an emerging approach for harvesting energy from the living environment. But its performance is limited by the maximum density of surface charges created by contact electrification. Here, by rationally designing a synchronous rotation structure, a charge pumping strategy is realized for the first time in a rotary sliding TENGs, which is demonstrated to enhance the charge density by a factor of 9, setting up a record for rotary TENGs. The average power is boosted by more than 15 times compared with normal TENGs, achieving an ultrahigh average power density of 1.66 kW $m^{-3}$, under a low drive frequency of 2 Hz. Moreover, the charge pumping mechanism enables decoupling of bound charge generation and the severity of interfacial friction in the main TENG, allowing surface lubricants to be applied for suppressing abrasion and lowering heat generation. The adaptability of the strategy to rotation and sliding type TENGs in low-frequency agitations provides a breakthrough to the bottleneck of power output for mechanical energy harvesting, and should have a great impact on high-power TENG design and practical applications in various fields.**

## 1. Introduction

The rapid development of internet of things, sensor networks, and wearable electronics imposes great importance on the facility and reliability of power supply.[1] The widely adopted battery is tethered by replacement and recharging, and its lifecycle is unfriendly to the environment.[2] As an alternative choice, triboelectric nanogenerators (TENGs), which are based on contact electrification and electrostatic induction, provide a promising approach by harvesting local mechanical energy to generate electricity, enabling self-powered systems that can be completely free of maintenance.[3] Compared to other energy harvesting techniques, the TENG has merits of low cost, versatile choices of materials and structures, light weight, and superiority in low-frequency energy harvesting.[4] Since its invention in 2012, enormous progresses have been made for demonstrating its potential application in self-powered sensing, micro/nanopower, blue energy harvesting, and high-voltage power.[5] Further development of the TENG relies greatly on the enhancement of the output power, which is highly dependent on the density of surface charges created by contact electrification.[6]

Generally, the charge density is mainly affected by material property, device structure, and environment condition, and couples tightly with the interfacial friction.[7] Hence violent friction is always needed for generating high charge density, which can cause severe abrasion and heat generation. Recently, through material optimization, corona charging, and suppressing air breakdown, the charge density was gradually improved, and reached 1003 μC $m^{-2}$ in a high vacuum condition for a contact-separation mode TENG.[7c,8] However, a series of problems arise with these approaches, such as complicated fabrication process, strict environment requirement, or poor stability. In 2018, the emergence of charge pumping mechanism provides a new strategy to improve the charge density, achieving 1020 μC $m^{-2}$ in ambient conditions.[9] The charge pumping mechanism is based on a floating conductive layer and injected bound charges from a charge pump, which can decouple the charge density and the intensity of friction. So far, the charge pumping mechanism is only realized for the contact-separation mode TENG. For other types of TENGs, whether the charge pumping mechanism can be available is still unknown. The rotary sliding TENG is a high performance design among TENG structures and is more adaptive to many forms of mechanical agitations.[5b,10] Thus, a realization of rotary charge pumping mechanism is very important for developing high performance TENGs toward practical applications.

In this work, a charge pumping strategy for rotation and sliding type TENG is demonstrated for the first time to boost the output performance. An as-fabricated rotary charge pumping triboelectric nanogenerator (RC-TENG) adopts a novel synchronous rotation structure that allows direct injection of bound charges from the pumping TENG to the main

Y. Bai, Dr. L. Xu, Dr. S. Lin, Dr. J. Luo, H. Qin, K. Han, Prof. Z. L. Wang
CAS Center for Excellence in Nanoscience
Beijing Key Laboratory of Micro-Nano Energy and Sensor
Beijing Institute of Nanoenergy and Nanosystems
Chinese Academy of Sciences
Beijing 100083, China
E-mail: zhong.wang@mse.gatech.edu

Y. Bai, Dr. L. Xu, Dr. S. Lin, Dr. J. Luo, H. Qin, K. Han, Prof. Z. L. Wang
School of Nanoscience and Technology
University of Chinese Academy of Sciences
Beijing 100049, China

Prof. Z. L. Wang
School of Materials Science and Engineering
Georgia Institute of Technology
Atlanta, GA 30332, USA

The ORCID identification number(s) for the author(s) of this article can be found under https://doi.org/10.1002/aenm.202000605.

**DOI: 10.1002/aenm.202000605**

 

TENG. With ultrafast accumulation of bound charges that can saturate in less than 1 s, the charge density is greatly boosted in ambient conditions, achieving an enhancement by a factor of 9 compared with normal TENGs. Moreover, the expandability of the RC-TENG enables multiple main TENGs charged by the pumping TENG simultaneously. With four main TENGs integrated, an ultrahigh maximum peak power of 658 mW and average power of 225 mW can be delivered under a low drive frequency of 2 Hz. Decoupling of surface charge generation and the severity of friction by the charge pumping strategy enables lubricants to be applied to enhance the durability. The successful combination of charge pumping mechanism with rotation and sliding type TENGs provides an ideal solution to the bottleneck of power output for mechanical energy harvesting in low-frequency range, and should have great impact on high-power TENG design and practical applications in various fields.

## 2. Results and Discussion

### 2.1. Device Structure and Working Principle

**Figure 1**a schematically shows the structure of the RC-TENG. The device is an integration of two major parts: pumping TENG and main TENG, each of which has two disks that act

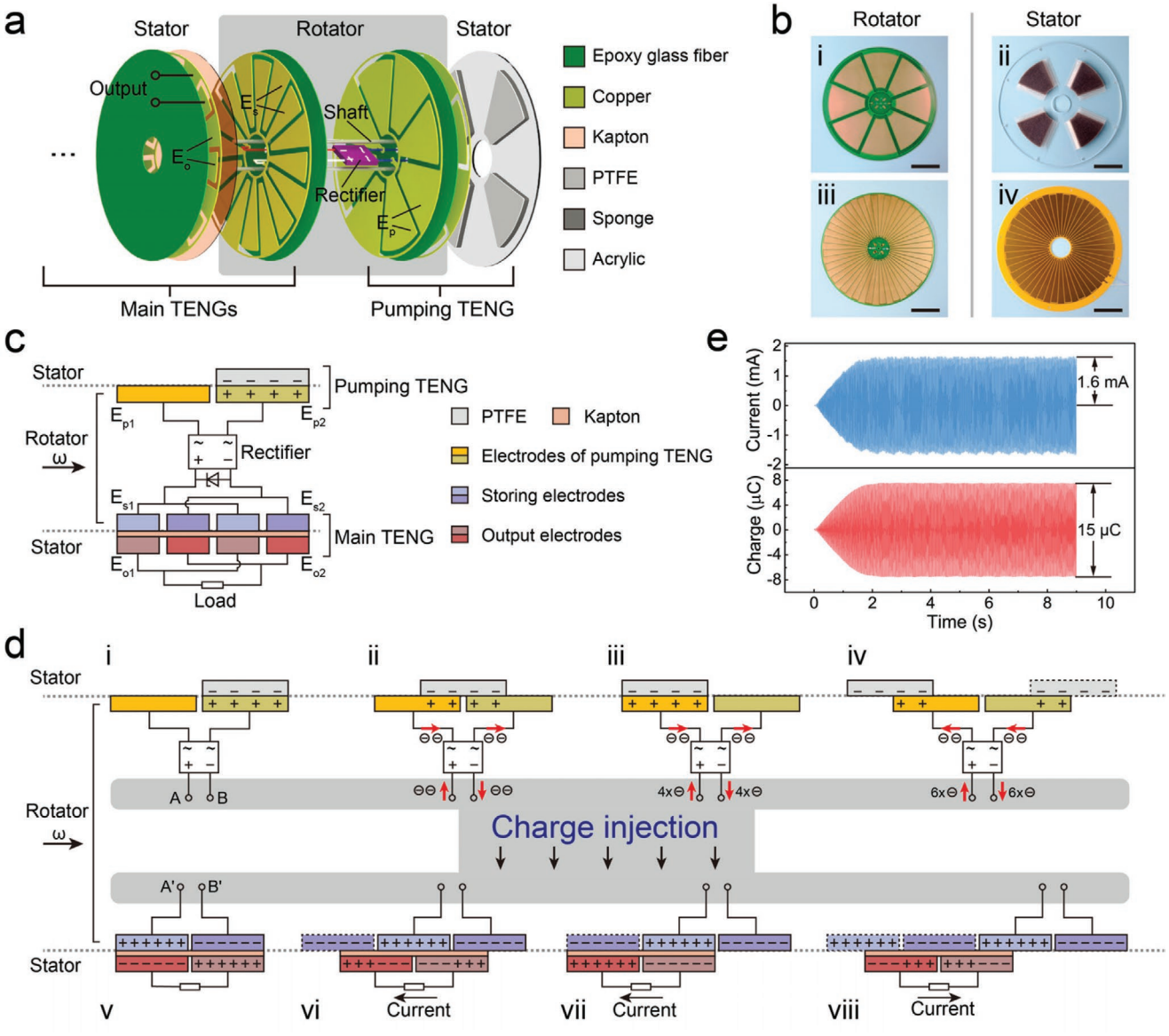


**Figure 1.** Structure and working principle of the rotary charge pumping triboelectric nanogenerator (RC-TENG). a) Schematic explosive view for the structure and materials of the RC-TENG. b) Photographs of the i) rotator and ii) the stator of the pumping TENG, iii) the rotator and iv) the stator of the main TENG. Scale bar, 5 cm. c) Schematic for circuit connection of the RC-TENG. d) i–iv) Working principle of the pumping TENG, and v–viii) working principle of the main TENG when the injected bound charges on $E_s$ reaches saturation. The Zener diode is not shown here. e) Typical short-circuit current and transferred charges of the device when four main TENGs are supplied by one pair of pumping TENGs.

as the rotator and the stator, respectively. Three types of functional electrodes are designed on such disks, namely electrodes of the pumping TENG ($E_p$) for supplying bound charges to the main TENG, electrodes for storing bound charges ($E_s$) on the rotator of the main TENG, and electrodes for electric energy output ($E_o$) on the stator of the main TENG. Here, $E_p$ and $E_s$ are connected by a rectifier whose direct current (DC) terminal is wired to $E_s$. For normal rotary TENGs, the electrode is usually arranged on the stator to avoid wire-twisting problems. In contrary, an inversion structure is adopted here to allow the disk of $E_p$ to rotate, and the rotator disks of the pumping TENG and the main TENG are assembled together by a group of shafts to form the total rotator of the whole device. In this arrangement, $E_p$ and $E_s$, together with the rectifier, can rotate in a novel synchronous mode. Charges from $E_p$ of the pumping TENG can be effectively injected into $E_s$ of the main TENG based on this facile and robust configuration without an extra brush and slip ring. Moreover, the design is easy for expanding, as shown in Figure S1 (Supporting Information). With multiple main TENGs supplied by the pumping TENG, the output can be further boosted.

The detailed structure of the pumping TENG is similar to the normal rotary TENG except the inversion configuration.[5b,10a] For the rotator of the pumping TENG, a pair of $E_p$ electrodes with complementary sectors are coated on a round epoxy glass fiber sheet through printed circuit board (PCB) techniques. For the stator, four sector-shaped polytetrafluoroethylene (PTFE) films are placed concentrically and uniformly on a round acrylic substrate. The sponge under the PTFE film ensures good contact between the rotator and the stator. All of the sectors have the same central angel of about 45° for periodical output. Moreover, the rotator disk of the pumping TENG can be coated with $E_p$ electrodes on both sides, forming a pair of pumping TENGs with an extra stator disk, as shown in Figure S1 (Supporting Information).

As for the main TENG, a pair of $E_s$ electrodes and another pair of $E_o$ electrodes are fabricated on the rotator and the stator, respectively, which have the same pattern of 48 complementary sectors with a central angel of about 7.5°. A layer of kapton film is adopted for insulation between the rotator and the stator of the main TENG. As charged $E_s$ will induce a high electric field, adhering the kapton film on the rotator could lead to excessive surface polarization on the film due to its relative static state to the $E_s$ electrodes, which would further cause output attenuation by shielding the opposite bound charges in $E_s$. Thus, the kapton film is adhered on the stator, and the electric field from $E_s$ on each area of the kapton film is alternating due to relative rotation, suppressing excessive surface polarization of the dielectric film. Photographs of the fabricated rotators and stators are shown in Figure 1b.

Figure 1c schematically demonstrates the fundamental circuit connection of the RC-TENG by a partial cross sectional view. The shown rectifier is used to convert alternate current (AC) output of $E_{p1}$ and $E_{p2}$ to DC signal, injecting positive and negative charges into $E_{s1}$ and $E_{s2}$, respectively. However, too much accumulated charges could lead to dielectric breakdown between $E_{s1}$ and $E_{s2}$, thus a Zener diode is applied to stabilize the voltage and provide a leakage channel for excessive charges. $E_{o1}$ and $E_{o2}$ on the stator of the main TENG are connected to the load to output generated electricity.

Figure 1d illustrates the detailed working principle of the RC-TENG. The pumping TENG roughly operates like a normal rotary sliding TENG,[5b,10a] where the coated Cu layer on the rotator acts as both triboelectric layer and inductive electrodes (Figure 1di–iv). During rotational sliding, the PTFE films are negatively charged due to triboelectrification, and corresponding positive charges in the Cu layer will always follow the motion of the PTFE films to screen the potential difference. The induced periodically transferred charges between $E_{p1}$ and $E_{p2}$ produce AC output to the rectifier, which converts the output to a DC form for continuously injecting charges to $E_s$ of the main TENG. More specifically, positive charges are injected into $E_{s1}$ and negative charges are injected into $E_{s2}$. Charges are accumulated during time in $E_s$ until reaching a balance with the leakage through the Zener diode (not shown in this figure). The bound charges in $E_{s1}$ or $E_{s2}$ will induce opposite charges in the underlying output electrodes. With the rotational sliding of $E_s$, the induced charges in $E_o$ will also follow the motion of the bound charges in $E_s$. Thus periodically transferring of charges can occur between $E_{o1}$ and $E_{o2}$, generating AC current in the connected load (Figure 1dv–viii). Actually, the mechanism shown here is also valid for the linear sliding type TENG, where the two parts will have relative motion in reciprocating mode, providing a universal charge pumping strategy for rotation and sliding type TENGs.

The charge pumping mechanism enables decoupling of bound charge generation and the severity of interfacial friction in the main TENG, and the temporal accumulating strategy imposes fewer requirements on the output of the pumping TENG, where smaller output can be compensated by longer time to reach the saturation level. In this way, the density of bound charges can be greatly enhanced and is only subjected to the dielectric strength of the system (if the protection Zener diode is not considered). Thus the output of the TENG can be further boosted. Moreover, through decoupling of surface charge generation and the severity of friction, the strategy enables less friction in the sliding interface and using lubricant in the main TENG, which can lower heat generation and suppress abrasion, improving the durability of the device.

Figure 1e shows typical short-circuit current ($I_{sc}$) and transferred charges ($\Delta Q$) of the RC-TENG when four main TENGs are supplied by one pair of pumping TENGs under a low drive frequency of 2 Hz. The $I_{sc}$ and $\Delta Q$ reach 1.6 mA and 15 μC, respectively. Considering the $\Delta Q$ of previous rotary TENGs is normally less than 1 μC for one TENG,[5b,10a] the boosted output of the RC-TENG represents a great advance toward practical high-power applications based on new mechanisms.

### 2.2. Performance Characterization

Generally, the injection of charges into $E_s$ of the main TENG is similar to charging a capacitor, though the capacitance between $E_{s1}$ and $E_{s2}$ should vary slightly during relative motion with $E_o$.[11] For higher voltage between $E_{s1}$ and $E_{s2}$, more charges will be bound in $E_s$ and better output can be expected. To accurately characterize the performance of the main TENG with injected charges at certain voltage, a commercial voltage source was applied first to provide a controllable and stable voltage

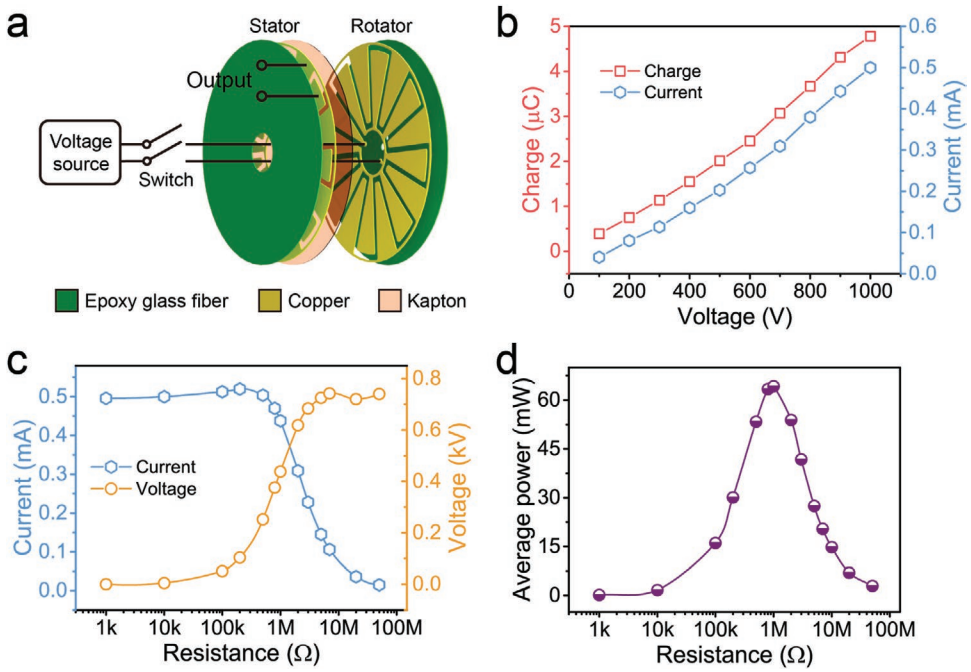


**Figure 2.** Output performance of the main TENG charged by a voltage source. a) Schematic for circuit connection of the testing. b) The transferred charges and short-circuit current of the main TENG when different voltages are applied. c) The peak current and peak voltage when various resistances are connected to the main TENG. d) The average power of the main TENG with various resistances. (b–d) were tested under a drive frequency of 2 Hz. (c,d) were tested when 1000 V are maintained on storing electrodes of the rotator by the voltage source.

between $E_{s1}$ and $E_{s2}$, instead of the pumping TENG (**Figure 2**a). Figure 2b shows the $\Delta Q$ and $I_{sc}$ of the main TENG when the applied voltage varies from 100 to 1000 V. The $\Delta Q$ and $I_{sc}$ present an approximately linear growth, from 0.4 to 4.8 μC and from 0.04 to 0.5 mA, respectively. The above results clearly show that higher voltage leads to higher output. However, too high a voltage will cause breakdown of the dielectrics, inducing sudden release of bound charges and the working state of the device can be very unstable. Thus, a trade-off is needed and the voltage should be controlled to saturate at a reasonable level with the Zener diode for the RC-TENG.

Figure 2c,d shows the dependence of the peak current, peak voltage, and output power of the main TENG on different resistances when a voltage of 1000 V is maintained on $E_s$. With load resistance increasing, the peak current decreases as a result of ohmic loss. Under high loads of dozens of megaohms, the output voltage attains about 740 V. A maximum average power of 64 mW can be achieved under a resistance of about 1 MΩ. The average power, which can reflect the continuous powering capability of the device, is calculated according to the following equation

$$P_{ave} = \frac{\int_0^T I^2 R \, dt}{T} \quad (1)$$

where $I$ is the output current, $T$ is the period, and $R$ is the load. Figure S2 (Supporting Information) shows the decay of $\Delta Q$ and $I_{sc}$ of the main TENG when the voltage (1000 V) supplied by the voltage source is removed. Both the $I_{sc}$ and $\Delta Q$ decay to almost zero in 5 s, showing leakage of the bound charges in the system. The exposed Cu electrodes on the rotator may be the reason for the leakage. When the voltage on the exposed electrodes is maintained at a high level, charge transfer from the exposed electrodes to the dielectric film in contact can occur, resulting in the leakage of the bound charges in the electrodes. Therefore, the performance of the device could be further enhanced by suppressing the leakage in the future.

As the source of bound charges in practical devices, the performance of the pumping TENG is important for the RC-TENG. More specifically, the transferred charges dictates the rate of injecting charges under certain rotation speed, and the open-circuit voltage affects whether the voltage in $E_s$ can be charged high enough. In the experiments here, one rotator with $E_p$ electrodes on both sides and two symmetrically placed stators form a pair of pumping TENGs, whose outputs are parallel connected to supply bound charges for the main TENG (Figure S1, Supporting Information).

The output performance of the pair of pumping TENGs is characterized, as shown in **Figure 3**. Figure 3a presents $\Delta Q$ and $I_{sc}$ of the parallel-connected pumping TENGs under drive frequencies ranging from 0.67 to 2.33 Hz. The $\Delta Q$ keeps stable around 1 μC, and the $I_{sc}$ increases linearly from 6.7 to 25.0 μA with rising drive frequencies owing to the relation $I = dQ/dt$. Figure 3b–d presents detailed curves of the open-circuit voltage ($V_{oc}$), $\Delta Q$, and $I_{sc}$ of the pair of pumping TENGs under a low drive frequency of about 2 Hz, respectively. The peak-to-peak value of $V_{oc}$ is 5.5 kV, which is capable to pump charges to the $E_s$ until a high voltage. The peak values of $\Delta Q$ and $I_{sc}$ for two pumping TENGs are 1.08 μC and 20 μA respectively. The frequency of the electrical output is several times of the drive frequency due to the radial grating structure of the rotator and stator.[5b,10a] The sector number of the pumping TENG affects

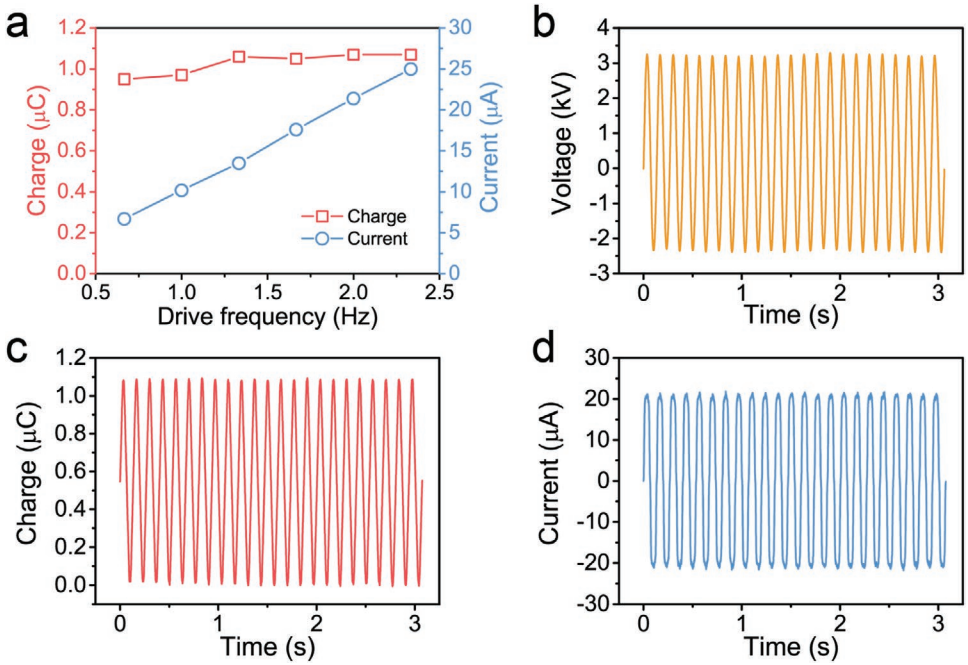


**Figure 3.** Output performance of one pair of parallel-connected pumping TENGs. a) The transferred charges and short-circuit current of the pumping TENGs under different drive frequencies. The curves for b) open-circuit voltage, c) transferred charges, and d) short-circuit current of the pumping TENGs under a drive frequency of 2 Hz.

the charge injection from two different aspects: the amount of transferred charges and the output voltage. With more sectors, more charges can be output from the pumping TENG in one round of rotation which can accelerate the charge injection, and the voltage of the pumping TENG should be decreased which will reduce the output of the main TENG if the voltage is lower than the stabilizing voltage of the Zener diode.

With the injected bound charges from the pair of pumping TENGs, the output performance of the RC-TENG incorporating one main TENG (noted as RC-TENG(1-M)) is investigated. A Zener diode was chosen to control the voltage of $E_s$ at a reasonable level just under the threshold breakdown voltage of the main TENG to maximize the output. **Figure 4**a shows the $\Delta Q$ and $I_{sc}$ of the RC-TENG(1-M) under different drive frequencies. The $I_{sc}$ presents linear relationship with the drive frequency, while $\Delta Q$ has a slight enhancement. Figure 4b presents the charging time of the RC-TENG(1-M) under different drive frequencies. Here, the charging time is defined as the time needed to reach 80% of the maximum value of $\Delta Q$ from zero, as shown in Figure S3 (Supporting Information). Higher drive frequencies can effectively shorten the charging time, which is less than 0.3 s under a drive frequency of 2 Hz.

The detailed curves of $\Delta Q$ and $I_{sc}$ for the RC-TENG(1-M) with a drive frequency of 2 Hz are shown in Figure 4c,d respectively, and the enlarged view from the beginning is presented in Figure S4 (Supporting Information). The $\Delta Q$ and $I_{sc}$ both increase fast from zero and saturate in about 0.5 s. The $\Delta Q$ can reach 4.5 μC, and such high transferred charges enable a large $I_{sc}$ of 0.47 mA under a low drive frequency. A normal rotary sliding TENG with similar structure was also fabricated for comparison, as shown in Figure S5 (Supporting Information). The normal TENG under the same agitation frequency and contact area can achieve transferred charges of 0.5 μC (Figure S6, Supporting Information), which indicates that the charge density in the main TENG is boosted by nine times. Table S1 (Supporting Information) further compares the output of the RC-TENG(1-M) and typical rotary sliding TENGs reported previously.[5b,10a] For traditional rotary sliding TENGs, higher drive frequencies or more sectors are demanded for larger current output due to poor transferred charges, which are normally less than 1 μC. The RC-TENG shows greatly boosted charge output, ready for high performance energy harvesting and practical applications.

A comparison between the injected charges from the pumping TENGs and the total output charges of the main TENG in the initial 1 s is shown in Figure 4e. A small amount of injected charges of 3.4 μC produce high total output charges of about 300 μC for the RC-TENG(1-M), demonstrating the superiority of applying charge pumping mechanism in rotary sliding TENGs. Figure 4f shows the average power of the RC-TENG(1-M) under different resistances. A maximum average power of 78 mW can be achieved under a low drive frequency of 2 Hz, which corresponds to an average power density of 1.66 kW $m^{-3}$, considering each main TENG occupies a volume of about 47.1 $cm^3$ (Due to that the electrode can be coated on both sides, the thickness of each main TENG is estimated as 1.5 mm). Because the power output is highly relied on the drive frequency and the grating number of the electrode, to evaluate the power enhancement, the power of the normal rotary TENG with similar structure and agitation frequency was tested (Figure S5, Supporting Information), and an average power of 5 mW can be obtained (Figure S7, Supporting Information). Hence the main TENG is demonstrated to enhance the average power by a factor of about 15 compared with the normal

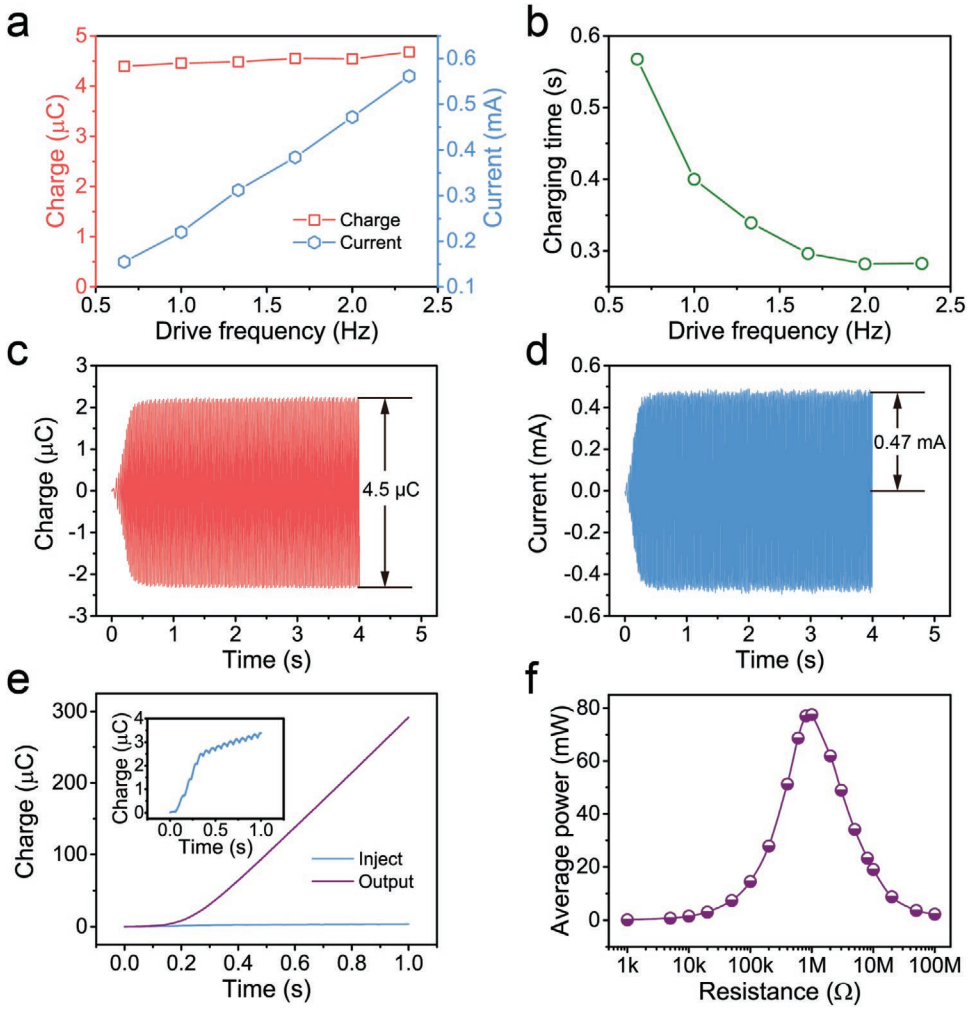


**Figure 4.** Output performance of one main TENG charged by a single pair of pumping TENGs. a) The transferred charges and short-circuit current of the RC-TENG(1-M) under different drive frequencies. b) The charging time of one main TENG under different drive frequencies. The curves for c) transferred charges and d) short-circuit current of the RC-TENG(1-M). e) The injected charges from the pumping TENGs and the total output charges of the main TENG in 1 s. Inset shows enlarged view of the injected charges of the pumping TENGs. f) The average power of the RC-TENG(1-M) under various resistances. The drive frequency is 2 Hz unless otherwise specified.

TENG. Besides, although the device is driven by regular agitations for characterization here, it can also harvest energy from irregular sources with high performance based on the reliability of the mechanical structure and the fast saturation capability.

Even higher output can be realized by a compact structure of integrating more parallel-connected main TENGs in the device, as shown in Figure S1 (Supporting Information). The output performance of the RC-TENG(4-M) consisting of four main TENGs (marked with a, b, c,d) and a pair of pumping TENGs (marked with a′,b′) is characterized (Video S1, Supporting Information). **Figure 5**a presents the $\Delta Q$ and $I_{sc}$ of each main TENG in the RC-TENG(4-M). An average $\Delta Q$ of 4.6 μC and $I_{sc}$ of 0.5 mA are obtained, respectively. Figure 5b shows the $\Delta Q$ and $I_{sc}$ for different numbers of main TENGs connected in parallel. With more main TENGs, the $\Delta Q$ and $I_{sc}$ increase almost linearly, and attain 15 μC and 1.6 mA, respectively for four main TENGs. The dependence of charging time on the number of main TENGs is shown in Figure 5c, and linear relationship can be observed. Only 1.3 s are needed to reach 80% of maximum transferred charges for four main TENGs, demonstrating fast saturation even with a large number of main TENGs.

Figure 5d presents the peak current, peak power, and average power of the RC-TENG(4-M) under loads of different resistances. The maximum peak power and average power are boosted to 658 and 225 mW, respectively, with a low matched resistance of about 500 kΩ. To further demonstrate the high output performance of the RC-TENG(4-M), two large capacitors are charged by the device with rectification, and the charging curves are shown in Figure 5e. The large capacitor of 1 mF can be fast charged to 6 V in 6.0 s from the initial state when no bound charges exist in the main TENGs. Thus the charging rate should be even higher when the main TENGs reach saturated level.

The exceptionally high output of the RC-TENG can be directly adopted to drive high-power electronic devices, which

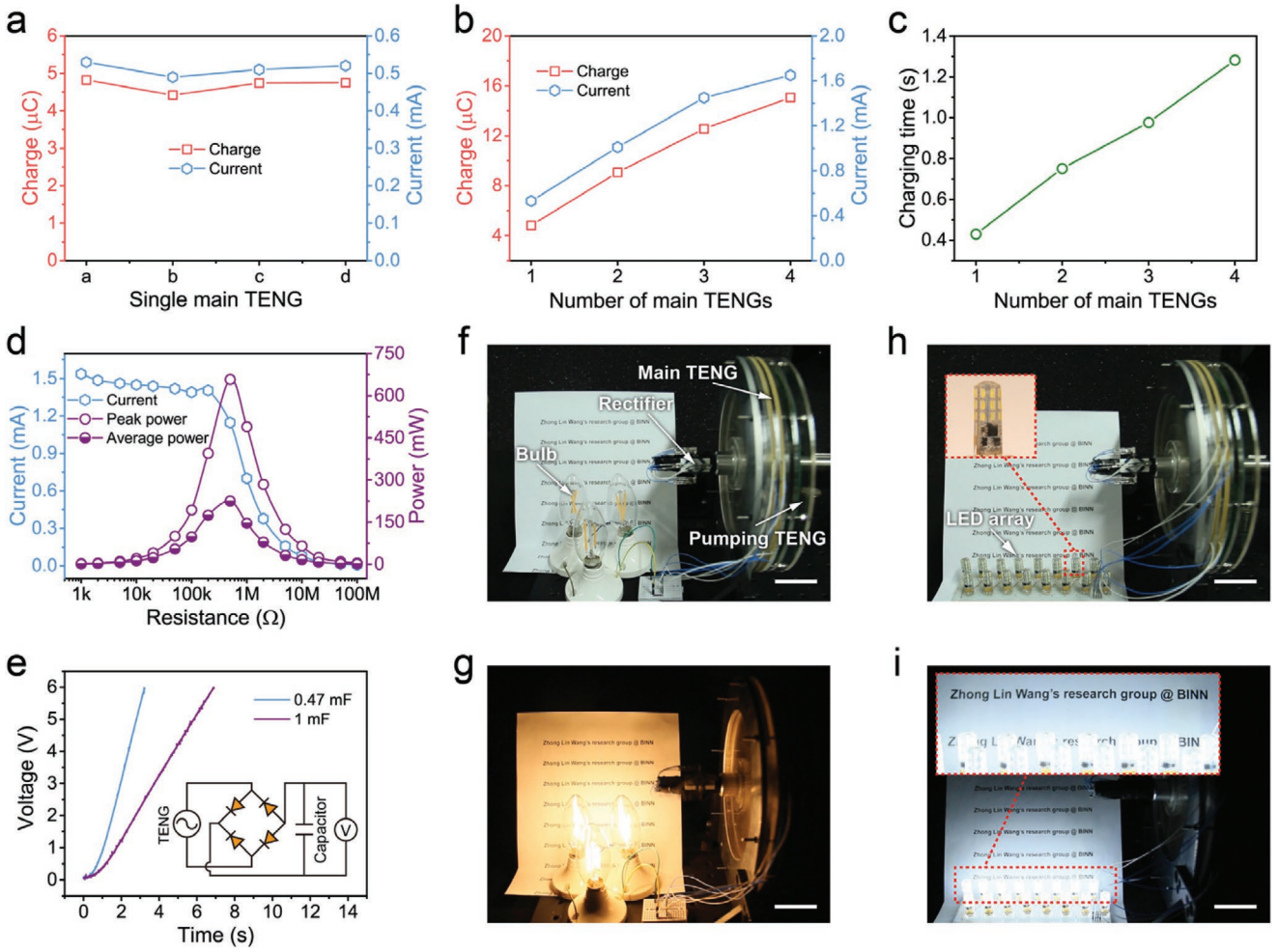


**Figure 5.** Output performance of four main TENGs charged by a single pair of pumping TENGs. a) The transferred charges and short-circuit current of each main TENG. b) The transferred charges and short-circuit current of different numbers of parallel-connected main TENGs. c) The charging time for different numbers of parallel-connected main TENGs. d) Dependence of the peak current, peak power, and average power of the RC-TENG(4-M) on different resistances. e) The voltage of the capacitors charged by the RC-TENG(4-M). Inset shows the circuit diagram. f) Setup of the RC-TENG(4-M) powering three large light bulbs. g) Three large bulbs are directly lighted by the RC-TENG(4-M). h) Setup of the RC-TENG(4-M) powering a LED array. Enlarged photograph shows a single LED lamp. i) The LED array is directly powered by the RC-TENG(4-M). Enlarged photograph shows that the printed text is illuminated by the LED array. Drive frequency, 2 Hz; scale bar, 5 cm.

used to be a tough task for normal TENGs under low agitation frequencies. As an intuitive demonstration, three large commercial light bulbs (rated power 2 W for each bulb) connected in series are powered by the RC-TENG(4-M) (Figure 5f,g and Video S2, Supporting Information). The light of the bulbs is strong enough for reading in complete darkness. Figure 5h presents another setup for the RC-TENG(4-M) to power a light emitting diode (LED) array, which consists of 16 LED lamps with 24 LED beads in each lamp, as shown in the inset of Figure 5h. Figure 5i and Video S3 (Supporting Information) present the lighted LED array and the printed text is fully illuminated. Adopting a parallel capacitor, the RC-TENG can supply power to electronics with nearly direct current output.[12] Such high output of the RC-TENG can be applied for various self-powered systems with greatly enhanced performance and large-scale environment energy harvesting, such as blue energy.[3d,e]

## 3. Conclusions

In this work, a charge pumping strategy for rotation and sliding type TENGs is demonstrated for the first time to boost the output performance, enabling decoupling of bound charge generation and the severity of interfacial friction. The as-fabricated RC-TENG adopts a novel synchronous rotation strategy which allows direct injection of bound charges from the pumping TENG to the main TENG for greatly enhancing the charge density. High transferred charges of about 4.5 μC for single main TENG is achieved in ambient conditions, and the average power is boosted for more than 15 times compared with normal TENGs, achieving an ultrahigh power density of 1.66 kW $m^{-3}$, under a low drive frequency of 2 Hz. Moreover, the performance of the RC-TENG can be further enhanced by compactly integrating multiple main TENGs due to its excellent expandability. With four main TENGs integrated,

an ultrahigh maximum peak power of 658 mW and average power of 225 mW can be delivered under 2 Hz driving. Meanwhile, the charge pumping mechanism enables decoupling of bound charge generation and the severity of interfacial friction in the main TENG, allowing surface lubricants to be applied for suppressing abrasion and lowering heat generation. The adaptability of the strategy to rotation and sliding type TENGs in low-frequency agitations provides an ideal solution to break through the bottleneck of power output for mechanical energy harvesting, and could pave the way toward high-power self-powered systems and large-scale environment energy harvesting.

## 4. Experimental Section

*Fabrication of the Main TENG*: The substrates of both the stator and rotator were epoxy glass fiber sheets (1 mm in thickness). Electrode layers of copper (35 µm in thickness) with complementary sectors (48 sectors in all) that have the same central angle of about 7.5° were coated on the substrate through PCB techniques. For the stator, a layer of kapton film (50 µm in thickness) was adhered on the side facing the rotator for insulation, and an acrylic sheet (4 mm in thickness) was applied for reinforcing the substrate, which can be removed in large-scale integration. Then, a thin layer of boron nitride lubricant (LRA-15) was sprayed on the rotator to reduce friction.

*Fabrication of the Pumping TENG*: For the rotator, electrode layers of copper (35 µm in thickness) with complementary sectors (eight sectors in all) that have the same central angle of about 45° were coated on both sides of a round epoxy glass fiber sheet (1 mm in thickness) through PCB techniques. For the stator, an acrylic sheet (4 mm in thickness) was shaped by a laser cutter (PLS6.75). Four sector-shaped sponges (5 mm in thickness) were adhered concentrically and uniformly on the acrylic as a buffer. Then, a layer of PTFE film (80 µm in thickness) was adhered on each sponge as the triboelectric layer.

*Integration of the Pumping TENG and the Main TENG*: All the stators had a diameter of 22 cm with a center hole of 3.5 cm, and all the rotators had a diameter of 20 cm. Through holes of 3 mm were drilled on the edge of the stators for connection by bolts and spacers. Similarly, through holes were drilled around the center of the rotators, four of which were used for assembling the rotators by four shafts with spacers, and the spare through holes were applied for the wires and the rectifier to connect electrodes on the rotators of the pumping TENG and the main TENG. In this arrangement, the total rotator of the whole device will have no interference with the stator in rotation. A Zener diode (BYV26E) was adopted in the device to stabilize the voltage.

*Characterization*: The transferred charges and the current were measured by an electrometer (Keithley 6514). The data were collected by a data acquisition card (NI PCI-6259) and a LabVIEW program. The open-circuit voltage of the pumping TENG was measured by an electrostatic voltmeter (Trek 347). A high-voltage DC power supply (DW-P303-1ACF0) was used for the supply of a stable voltage. The amount of injected charges from the pumping TENG was measured by an electrometer connected in series with the rectifier (Figure S8, Supporting Information). The rotator of the TENG was driven by a motor (6IK200GU-S3/SF) and the rotation speed was directly read from the controller (Taili US).

## Supporting Information

Supporting Information is available from the Wiley Online Library or from the author.

## Acknowledgements

The research was supported by the National Key R & D Project from Minister of Science and Technology, China (No. 2016YFA0202704), National Natural Science Foundation of China (No. 51605033, 51432005), Youth Innovation Promotion Association, CAS (No. 2019170), and Beijing Municipal Science & Technology Commission (No. Z171100002017017).

## Conflict of Interest

The authors declare no conflict of interest.

## Author Contributions

Y.B. and L.X. contributed equally to this work. L.X. and Z.L.W. conceived the idea. L.X., Y.B., and S.L. designed the device. Y.B., S.L., and L.X. fabricated the device. Y.B., L.X., J.L., H.Q., and K.H. did the experiment. Y.B., L.X., and Z.L.W. discussed the data and prepared the manuscript. Z.L.W. guided the whole project.

## Keywords

charge pumps, high output, rotation, triboelectric nanogenerators

Received: February 16, 2020
Revised: March 22, 2020
Published online:

[1] a) D. Butler, *Nature* **2006**, *440*, 402; b) E. Borgia, *Comput. Commun.* **2014**, *54*, 1; c) S. Wang, J. Xu, W. Wang, G. N. Wang, R. Rastak, F. Molina-Lopez, J. W. Chung, S. Niu, V. R. Feig, J. Lopez, T. Lei, S. K. Kwon, Y. Kim, A. M. Foudeh, A. Ehrlich, A. Gasperini, Y. Yun, B. Murmann, J. B. Tok, Z. Bao, *Nature* **2018**, *555*, 83; d) W. Gao, S. Emaminejad, H. Y. Y. Nyein, S. Challa, K. Chen, A. Peck, H. M. Fahad, H. Ota, H. Shiraki, D. Kiriya, D. H. Lien, G. A. Brooks, R. W. Davis, A. Javey, *Nature* **2016**, *529*, 509; e) D. H. Kim, N. Lu, R. Ma, Y. S. Kim, R. H. Kim, S. Wang, J. Wu, S. M. Won, H. Tao, A. Islam, K. J. Yu, T. I. Kim, R. Chowdhury, M. Ying, L. Xu, M. Li, H. J. Chung, H. Keum, M. McCormick, P. Liu, Y. W. Zhang, F. G. Omenetto, Y. Huang, T. Coleman, J. A. Rogers, *Science* **2011**, *333*, 838.

[2] D. Larcher, J. M. Tarascon, *Nat. Chem.* **2015**, *7*, 19.

[3] a) F.-R. Fan, Z.-Q. Tian, Z. Lin Wang, *Nano Energy* **2012**, *1*, 328; b) J. Xiong, P. Cui, X. Chen, J. Wang, K. Parida, M. F. Lin, P. S. Lee, *Nat. Commun.* **2018**, *9*, 4280; c) Q. Zheng, Y. Zou, Y. Zhang, Z. Liu, B. Shi, X. Wang, Y. Jin, H. Ouyang, Z. Li, Z. L. Wang, *Sci. Adv.* **2016**, *2*, e1501478; d) Z. L. Wang, T. Jiang, L. Xu, *Nano Energy* **2017**, *39*, 9; e) C. Wu, A. C. Wang, W. Ding, H. Guo, Z. L. Wang, *Adv. Energy Mater.* **2019**, *9*, 1802906.

[4] a) Z. L. Wang, *Faraday Discuss.* **2014**, *176*, 447; b) Z. L. Wang, *Mater. Today* **2017**, *20*, 74; c) C. Zhang, W. Tang, C. Han, F. Fan, Z. L. Wang, *Adv. Mater.* **2014**, *26*, 3580; d) Y. Zi, H. Guo, Z. Wen, M. H. Yeh, C. Hu, Z. L. Wang, *ACS Nano* **2016**, *10*, 4797.

[5] a) J. Luo, Z. Wang, L. Xu, A. C. Wang, K. Han, T. Jiang, Q. Lai, Y. Bai, W. Tang, F. R. Fan, Z. L. Wang, *Nat. Commun.* **2019**, *10*, 5147; b) Y. Bai, L. Xu, C. He, L. Zhu, X. Yang, T. Jiang, J. Nie, W. Zhong, Z. L. Wang, *Nano Energy* **2019**, *66*, 104117; c) X. Yang, L. Xu, P. Lin, W. Zhong, Y. Bai, J. Luo, J. Chen, Z. L. Wang, *Nano Energy* **2019**, *60*, 404; d) Y. Bai, C. B. Han, C. He, G. Q. Gu, J. H. Nie, J. J. Shao, T. X. Xiao, C. R. Deng, Z. L. Wang, *Adv. Funct. Mater.* **2018**, *28*,

 

1706680; e) R. Hinchet, H. J. Yoon, H. Ryu, M. K. Kim, E. K. Choi, D. S. Kim, S. W. Kim, *Science* **2019**, *365*, 491; f) J. Nie, X. Chen, Z. L. Wang, *Adv. Funct. Mater.* **2019**, *29*, 1806351; g) L. Xu, H. Wu, G. Yao, L. Chen, X. Yang, B. Chen, X. Huang, W. Zhong, X. Chen, Z. Yin, Z. L. Wang, *ACS Nano* **2018**, *12*, 10262; h) X. Cao, Y. Jie, N. Wang, Z. L. Wang, *Adv. Energy Mater.* **2016**, *6*, 1600665.

[6] a) Y. Zi, S. Niu, J. Wang, Z. Wen, W. Tang, Z. L. Wang, *Nat. Commun.* **2015**, *6*, 8376; b) S. Wang, Y. Xie, S. Niu, L. Lin, C. Liu, Y. S. Zhou, Z. L. Wang, *Adv. Mater.* **2014**, *26*, 6720.

[7] a) W. Tang, T. Jiang, F. R. Fan, A. F. Yu, C. Zhang, X. Cao, Z. L. Wang, *Adv. Funct. Mater.* **2015**, *25*, 3718; b) H. Zou, Y. Zhang, L. Guo, P. Wang, X. He, G. Dai, H. Zheng, C. Chen, A. C. Wang, C. Xu, Z. L. Wang, *Nat. Commun.* **2019**, *10*, 1427; c) J. Wang, C. Wu, Y. Dai, Z. Zhao, A. Wang, T. Zhang, Z. L. Wang, *Nat. Commun.* **2017**, *8*, 88; d) A. Šutka, K. Mālnieks, L. Lapčinskis, P. Kaufelde, A. Linarts, A. Bērziņa, R. Zābels, V. Jurķāns, I. Gorņevs, J. Blūms, M. Knite, *Energy Environ. Sci.* **2019**, *12*, 2417.

[8] a) H. Y. Li, L. Su, S. Y. Kuang, C. F. Pan, G. Zhu, Z. L. Wang, *Adv. Funct. Mater.* **2015**, *25*, 5691; b) T. Zhou, L. Zhang, F. Xue, W. Tang, C. Zhang, Z. L. Wang, *Nano Res.* **2016**, *9*, 1442.

[9] L. Xu, T. Bu, X. Yang, C. Zhang, Z. L. Wang, *Nano Energy* **2018**, *49*, 625.

[10] a) G. Zhu, J. Chen, T. Zhang, Q. Jing, Z. L. Wang, *Nat. Commun.* **2014**, *5*, 3426; b) J. Cheng, W. Ding, Y. Zi, Y. Lu, L. Ji, F. Liu, C. Wu, Z. L. Wang, *Nat. Commun.* **2018**, *9*, 3733.

[11] S. Niu, Y. Liu, X. Chen, S. Wang, Y. S. Zhou, L. Lin, Y. Xie, Z. L. Wang, *Nano Energy* **2015**, *12*, 760.

[12] a) S. Niu, Y. S. Zhou, S. Wang, Y. Liu, L. Lin, Y. Bando, Z. L. Wang, *Nano Energy* **2014**, *8*, 150; b) J. Yoo, D. Yoo, S. Lee, J.-Y. Sim, W. Hwang, D. Choi, D. S. Kim, *Nano Energy* **2019**, *56*, 851.